Reactivity of Boron Nitride Nanomaterials with Phosphoric Acid and its Application in the

Purification of Boron Nitride Nanotubes

Kevin R. Shumard $^{\mathfrak{s},\,\mathcal{V}}$, Jesus A. I. Acapulco Jr. § , Matteo Pasquali $^{\mathfrak{s},\,\S}$, Angel A. Martí $^{\mathfrak{s},\,\perp}$, **

- ♪ Department of Chemistry, Smalley-Curl Institute, Rice University, 6100 Main Street, Houston, Texas 77005, United States
- § Department of Chemical and Biomolecular Engineering, Rice University, 6100 Main Street, Houston, Texas 77005, United States
- ─ Department of Materials Science and NanoEngineering, Rice University, 6100 Main Street,
 Houston, Texas 77005, United States
- | Smalley-Curl Institute for Nanoscale Science and Technology, Rice University, Houston, Texas 77005, USA

Abstract

Boron nitride nanotubes (BNNTs) offer compelling promise in 21st century materials, due to their high-tensile strength, thermal conductivity, chemical stability, and insulating properties. Current synthetic methods result in the formation of many non-nanotube byproduct structures with similar BN connectivity, which makes their removal difficult. As a result, there is considerable focus on developing purification methods that produce neat BNNTs. Here, we present a new purification process that removes impurities to produce BNNTs with high purity.

Employing the intercalating nature of phosphoric acid and taking advantage of the wet thermal etching of boron nitride, our strategy combines phosphoric and hydrochloric acids with samples containing a mixture of BN materials (such as BNNT and BN nanocages) inside a constant volume reaction setup in a furnace. The reaction removes impurities such as nanocages, hexagonal boron nitride (hBN), and less ordered BN material. Overall, this method can result in mass yields up to 29% purified material, a result that is highly dependent on the concentration of impurities in the starting material. This result is confirmed using scanning electron microscopy (SEM). Analysis using x-ray photoelectron spectroscopy (XPS), x-ray diffraction (XRD), and infrared spectroscopy (IR) demonstrate that there are not significant chemical changes to the BNNTs after the reaction, which produces BNNTS that are highly enriched and purified.

Introduction

Boron nitride nanotubes (BNNTs) are a unique material, analogous to carbon nanotubes (CNTs), with similarly interesting physical properties such as tensile strength, Young's modulus, and thermal conductivity. ^{1–5} In contrast to CNTs, BNNTs are insulators with a band gap around 5.7 eV and are much more thermally stable up to ca. 900 °C. ⁵ These properties are desirable for applications in different areas including biomedical imaging, ⁶ hydrogen storage, ⁷ and low-weight, high-strength materials, ⁸ among others.

BNNTs were first synthesized in 1995⁹ and have since been produced in a variety of different ways. Yet, scalable syntheses of pure BNNTs are yet to be developed, and most syntheses yield BNNTs with a variety of impurities. Given each synthesis method produces its own impurities, there are still outstanding challenges in the purification of BNNTs. 1,2,9–12 BNNTs are particularly chemically inert, and high temperatures or pressures (or both) are required to synthesize this

material in large quantities. These methods, consequently, result in a significant amount of non-nanotube material in the form of amorphous boron, hexagonal boron nitride (hBN), boron nitride cages, and other less ordered BN material. As a result, there is a considerable thrust to develop purification methods that result in neat BNNTs. Current methods have used processes including chemical etching, ^{13,14} functionalization, ^{15–17} or physical separation techniques ^{18–20} to eliminate the unwanted BN material from BNNTs.

There are several methods that can effectively remove amorphous boron, given that it can be easily converted into oxides that are soluble in water. 14 On the other hand, cages, hBN, and other BN materials are chemically similar to BNNTs, which therefore limits their selective removal.^{21,22} Wet-thermal etching has demonstrated that the removal of some of the unwanted species is possible. While the bond connectivity in hBN is similar to that of BNNTs, its morphology is different, which makes available a greater proportion of edges, vacancies, local defects, and reactive species that are exposed and thus are more reactive in a high-temperature steam environment.¹⁴ As a result, this method has become popular to remove some unwanted material. The challenge with this method is that it requires a highly specialized setup and temperatures that exceed 500 °C. In addition, while this method selectively removes non-BNNT impurities, it also removes tubes resulting in low yields (<5% for the purest material). 14 Due to the chemical similarities between species, there is not an agreed-upon method for the evaluation (quantitation) of the different BN species in a sample. As such, we refer to yields as a mass percentage of the remaining purified BN material, which is highly variable due to fluctuations in the composition of the starting material from batch to batch (e.g. ratio of cages vs BNNTs). This value nonetheless allows us to compare our results to others in the field that have used a similar definition.

In this study, we add a new chemical method to the toolbox of purification techniques for BNNTs that were synthesized using the high-temperature-pressure method (HTP). The raw material used in this research is >95% BN material (with elemental boron already being removed) by XPS (Table S1), which includes BNNTs, cages, h-BN, and amorphous boron nitride. Given that the impurities are BN material, we introduce an alternative purification method using a phosphoric/hydrochloric acid solution. It has been shown that phosphoric acid can intercalate hBN,²³ and also react with boron oxides to form BPO4. Given the particular chemical connectivity in BNNTs and BN cages (alternating B and N atoms), having a seamless sphere becomes challenging, resulting in unconnected atoms and defects in cages; notice that cylindrical structures such as BNNTs can seamlessly connect without restrictions. The paradigm here is that the higher concentration of defects, as a consequence of the restrictive connectivity that is present in amorphous and cage-like structures, provides labile sites for species such as phosphoric acid, allowing for selective etching.

Experimental Section

Constant-Volume Reaction Setup

Experiments were carried out in several stainless-steel PTFE-lined constant-volume reactor vessels with an interior space ranging from 20 to 100 mL. PTFE-lined reaction vessels are necessary, as stainless steel can react with acids to form more dangerous products such as chromic acid. A general experimental procedure started with 30 mg of BNNTs (labeled SP10R from BNNT LLC) dispersed in 10 mL dimethylformamide (DMF) and stirred for 30 minutes, followed by 2 minutes of sonication. This was done to separate tube bundles and individualize nanotubes as much as possible.²⁴ The resultant dispersion was then filtered (Sartorius PTFE

filter, 0.2 µm) and rinsed with 50 mL water to remove excess solvent. The filtrate was then redispersed in 10 mL phosphoric acid aqueous (or hydrochloric) solution and stirred again for 30 minutes followed by 2 minutes sonication. The dispersion was then placed inside the constant volume reactor and heated at various temperatures and times. Care was taken to ensure that the vessels were sealed tightly in order to remove the risk of rapid decompression. Furthermore, all vessels were rated to at least 3 MPa at 180 °C and all experimental conditions were calculated or measured to be lower than these parameters, with a general measurement around 0.5 MPa (0.4-0.6 MPa range). After heating was finished, the dispersion was placed in a 15 mL centrifuge tube and centrifuged at 4696 G for 30 minutes in a Sorvall ST16 centrifuge. It is important to allow the rotor to brake slowly in order to ensure the centrifuged material does not move. The supernatant was removed, and ca. 10 mL boiling water was added, mixed, and centrifuged again for 30 minutes. This process was repeated 3 times, and the pH checked to ensure neutral pH. This step is necessary to remove all excess reactant acid as well as produced boron phosphate and other oxides. The resultant material was dispersed in ca. 3 mL hot water, sonicated for 2 minutes, then frozen with liquid nitrogen and lyophilized overnight. Depending on the reaction conditions, the sedimented material consisted of enriched boron nitride nanotubes, crystalline (insoluble) boron phosphate, or some mixture of the two. It should be noted that it is possible that some purified material (likely smaller tubes) exists in the supernatant, though the centrifugation method resulted in the highest mass yields due to lower loss potentials when compared to vacuum filtration.

Experiments were performed by varying the phosphoric acid concentration, time, and temperature and were all conducted with a target of 3 mg/mL dispersions of BNNTs.

Nonetheless, we have been able to do this process at 5x scale (150 mg) with similar results, to

show the procedure can be scaled up. Furthermore, experiments were performed using various acids, organic solvents, and pH, as detailed in the Supporting Information (Figures S1-3).

Purification assessment was primarily based on qualitative morphology from imaging and mass yield in weight percent, as well as diffraction and spectroscopic techniques as described below.

Scanning Electron Microscopy

Dry samples of BNNTs are challenging to image, particularly if done without sputtering. In order to achieve true homogeneity of the sample and to ensure high-quality micrographs were attained, each sample was dispersed in methanol at 1 mg/mL concentration and sonicated for 2 minutes to ensure dispersion. Using either the bare aluminum SEM stub or a silicon wafer cut into 1 cm² pieces and carbon taped to an aluminum SEM stub, 50 μL of the dispersion were dynamically spin coated at 1000 rpm, and spun for 1 minute, followed by drying at 110 °C for at least 1 hour under vacuum. Imaging was done using a Helios NanoLab 600 with a field-emission gun. In order to maintain a pristine sample, no coating was added, even though BNNTs are non-conductive. To limit specimen charging and avoid additional artifacts, a low electron beam acceleration voltage of 1.0 kV and current between 6.3 and 50 pA was used. For high-resolution images (Figure S1) a minimal current of 0.78 pA was used to ensure minimum charging. Micrographs were taken at a low working distance of 2.0 to 3.0 mm using a through-lens secondary electron detector.

Transmission Electron Microscopy

Samples were prepared similarly to SEM samples at a concentration of 1 mg/mL in methanol. This was then diluted to 0.1 mg/mL in methanol. The resultant suspension was sonicated for 2 minutes, and a single drop was placed on a lacey-carbon grid (Ted Pella, Pelco) and allowed to

evaporate. The grids were then dried under vacuum overnight at 110 °C. Imaging was done at 200 kV using a Jeol 2100F TEM.

X-Ray Diffraction

X-Ray diffraction (XRD) patterns were obtained using a SmartLab II by Rigaku. Experiments were conducted using ca. 5 mg samples that were dried for at least 1 hour at 110 °C under vacuum to ensure residual water was removed. Each sample was ground into a powder and placed on a zero-background sample holder. The diffractions were captured from 15 to 80 degrees with a step size was 0.05 degrees and the dwell time was 1 min/deg, using Cu-K α (wavelength λ =1.54059 Å) as the X-ray source.

Infrared Spectroscopy

After lyophilization, the solid sample was dried for at least 1 hour at 110 °C under vacuum to remove traces of water. The samples were then placed onto an attenuated total reflectance (ATR) crystal and analyzed using Fourier transform infrared spectroscopy (FTIR) with a Nicolet FTIR iS50-FTIR. Samples were analyzed from 500-4000 cm⁻¹ with a step size of 4 cm⁻¹ and averaged over 32 scans. The spectra were then normalized to the BN longitudinal vibration mode at 1351 cm⁻¹.

X-Ray Photoelectron Spectroscopy

X-ray photoelectron spectroscopy (XPS) was conducted using a Phi-Quantera spectrophotometer. Samples were dried in a vacuum oven after lyophilization to ensure no excess water was present. Each sample was placed onto an aluminum strip and had a thickness of at least 0.5 mm to avoid substrate detection. An aluminum source with 45.3 W power and 200

μm spot size was used for each sample. An initial survey scan of the samples was conducted using a pass energy of 140 eV from binding energies 1100-0 eV, with a collection time of 80 ms and a step size of 0.5 eV. High-resolution scans used a pass energy of 26 eV with 200 ms collection time and step size of 0.1 eV. Deconvolution was performed using PHI Multipak (9.9.0.19). All spectra were shifted to match the C 1s peak at 284.8 eV for an accurate comparison of the samples. Due to the B 1s and P 2s overlap, the P 2p peak was used to determine the overall composition of phosphorus leftover due the use of phosphoric acid. All comparisons were done using literature values²⁵ or referenced using the Handbook of XPS,²⁶ or NIST tables.

Results and Discussion

Reaction Process

Inspired by the reported intercalation of phosphoric acid on hBN by the Mallouk group²³ and the known synthesis of boron phosphate from boric and phosphoric acids, we used phosphoric acid to remove BN impurities created during the BNNT synthesis. SEM analysis of the as-received material shows the morphology and abundance of BN cages in the sample (Figure 1a), the most common by-product in the synthesis of SP10R BNNTs (BNNT LLC). Unlike the analogous fullerenes, cages have many more morphologies and tend to be on the order of >150 nm, which makes them prominent in the micrographs, though it is assumed that smaller cages are present. One of the major challenges in the purification of BNNTs is that bundles trap impurities that will not be available for reaction or removal. The rationale is that given phosphoric acid's known intercalation within h-BN, it will be able to impregnate the material completely and then react

with defective boron sites to form amorphous boron phosphate, sparing pristine BNNTs.

Amorphous boron phosphate is soluble in water and easily removed from the mixture.

The as-received material (BNNT LLC SP10R) was treated by the manufacturer to remove elemental boron. XPS analysis of the material confirms that the as-received material is >95% BN, (Figure S2 and Table S1), which again includes BNNTs, cages, h-BN, and amorphous boron nitride. Previous studies indicate that BN materials can react with water to produce boric acid and ammonia (eq 1).¹⁴ This process is slow at low temperatures (<200 °C), however the equilibrium could be shifted if boric acid is removed, for example by its reaction with phosphoric acid to form boron phosphate (eq 2).^{27–30} Alternatively, the higher availability boron oxide defect sites could lead to the direct reaction of BN nanomaterials with phosphoric acid (eq 3). The mechanism for formation of boron phosphate is elusive, but previous studies have proposed that O-B-O and O-P-O groups of boric and phosphoric acids can react to form the BPO₄ network.³¹ While the formation of BPO4 is unclear in our synthesis, we propose that defect sites are largely populated with boron oxides which can interact with phosphoric acid to form extended BPO₄ networks (eq 2). Alternatively, exposed BN (as etching occurs) could react directly with phosphoric acid (eq 3) to form BPO₄. At lower concentrations of phosphoric acid, the BPO₄ remains amorphous, and thus, soluble in the reaction solution.

Scheme 1. Reactions that occur in the constant volume reactors with boron nitride and phosphoric acid.*

$$BN_{(s)} + 3H_2O_{(g)} \rightarrow B(OH)_{3(aq)} + NH_{3(g)}$$
 (eq 1)

$$B(OH)_{3(aq)} + H_3PO_{4(aq)} \rightarrow BPO_{4(s)} + 3H_2O_{(1)}$$
 (eq 2)

$$BN_{(s)} + H_3PO_{4(aq)} \rightarrow BPO_{4(s \text{ or } aq)} + NH3_{(g)}$$
 (eq 3)

*Species labeled as aqueous may be gaseous depending on the temperatures and pressures reached. Boron phosphate is insoluble in water when crystalline and soluble in water when amorphous. At low concentrations of H₃PO₄, BPO₄ remains amorphous.²⁵

In our first experiments, SP10R BNNTs were reacted with 85% phosphoric acid in a pressure autoclave at 150 °C for 24 hrs. Interestingly, when the material was analyzed after the reaction, we found tetrahedral crystals (Figure 1b), consistent with the crystal structure of boron phosphate. A close analysis of these images showed tubular structures on the surface of the crystals, which indicates that some BNNTs survived the reaction. It is also important to mention that no BN cages were found, and thus it can be concluded that cages reacted faster with phosphoric acid than BNNTs. Additional experiments were performed to demonstrate that several sources of boron would produce boron phosphate by using a constant volume reactor and the conditions previously described. Therefore, hBN and boric acid were tested and do indeed create boron phosphate particles, as shown in the Supporting Information (Figure S3). Interestingly, boric acid produces particles much smaller than BNNTs, while hBN produces particles that are much larger and show significant intergrowth. It is likely that the lamellar nature of hBN promotes crystal intergrowth. Based on these results we decided to explore the chemical space (time, temperature, and concentration of phosphoric acid) to find conditions that would lead to the preferential etching of BN cages, leaving BNNTs intact, without the formation of crystalline boron phosphate. The removal of cage impurities was studied from 100-300 °C with varying concentrations of phosphoric acid from 5-85% (w/w), see section below and supporting information Figures S3 and S5.

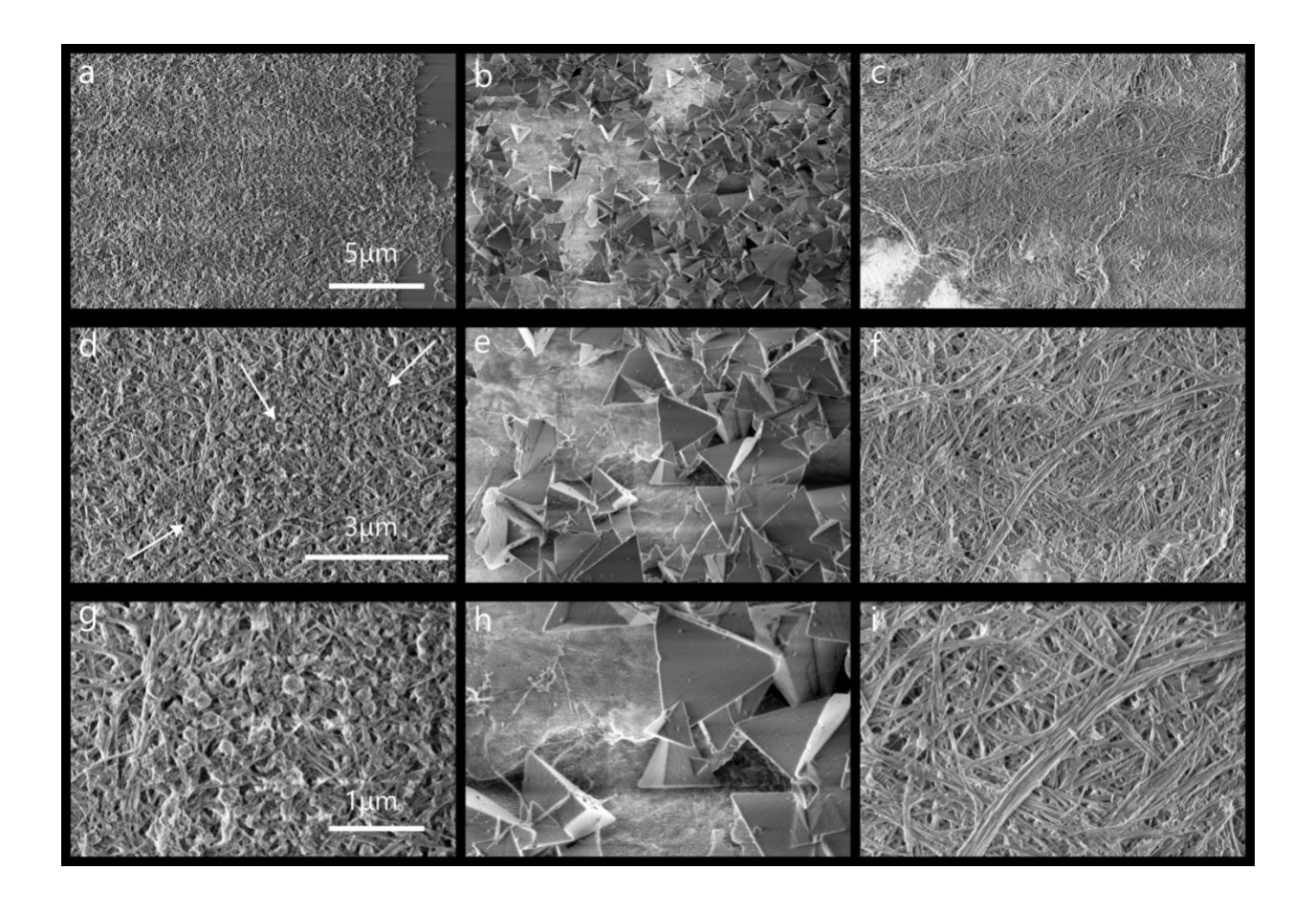


Figure 1. SEM micrographs of BNNT phosphoric acid isochoric experiments. Scale bars are for each row, while each column is increasing magnification. (a, d, g) Starting material. Arrows indicate impurities. (b, e, h) Tetrahedral boron phosphate nanoparticles from 85% (w/w) phosphoric acid. (c, f, i) Purified material at 25% (w/w) phosphoric acid.

Reaction optimization

Phosphoric acid-mediated tetrahedral boron phosphate nanoparticles were shown to be created whenever a significant amount and concentration of phosphoric acid was used, though many temperatures were found to favor the formation of these particles. Specifically, when the constant volume reaction was performed as low as 100 °C with 85% phosphoric acid solution, these particles still formed readily (Figure S3e). At concentrations 50% (w/w) of phosphoric acid

and 150 °C, fewer boron phosphate particles appeared, but they were still present (Figure S4f). In addition, when the 85% phosphoric acid solution was used in a simple reflux setup (thus not being isochoric, and at a temperature of about 154 °C), the reaction still created boron phosphate particles (Figure S3f). Interestingly, the particles were polydisperse when not in an isochoric setup. This could be related to the production of nucleation centers (bubbles) during reflux. Initially, we thought about chemically removing the BPO₄ crystals and leaving the purified tubes, however we found that these BPO₄ crystals were stable under a variety of conditions, and therefore we opted to tune the reaction to reduce the amount of BPO₄ crystals present in the sample at the end of the reaction.

Purification of tubes starts to occur around 50% (w/w) phosphoric acid (Figure S4f). Non-tube materials start to preferentially etch as low as 5% (w/w) phosphoric acid (Figure S4b), though the imbalance of etching tubes to impurities is not as apparent at lower concentrations. There is a narrow balance that is required to remove impurities from tubes at <50% (w/w) phosphoric acid. On the one hand, 50% will remove impurities, but also etches almost everything so that there is very little BNNT material left. On the other hand, at 5% (w/w) concentration of phosphoric acid, the amount is not enough to etch the material at an appropriate rate. At 25% (w/w), however, a proper balance is reached, where most of the impurities are removed, and around 7% mass yield is typically found (mass yields vary from 29% to less than 1% depending on the amount of impurities in the starting material). Of course, the yield is based on the concentration of impurities, which at this time is extremely difficult to quantify from sample to sample.

It is possible the reason the 25% (w/w) phosphoric acid concentration work best is related to the formation of amorphous boron phosphate instead of crystalline boron phosphate. It is proposed that at concentrations higher than 50% (w/w) the B-O-P connectivity readily forms and

propagates, which promotes extended crystalline structures. Whether this arises from larger aggregates forming in solution or if there is some 'scaffolding' on the BN structures during etching is unclear. Regardless, there is some nucleation process that is necessary to form extended B-O-P networks in a tetrahedral geometry. At concentrations below 50% (w/w) phosphoric acid, particles do not form as readily and around 25% (w/w) the formation of BPO4 crystalline particles is precluded. It is possible that by limiting the interaction of phosphoric acid and boric acid moieties at defects, (due to a lower concentration of phosphoric acid) only a small amount of boron phosphate is produced at a time and released from the BN material. These lower-ordered boron phosphate molecules aren't large enough to nucleate and promote crystallization. This mechanism is still under investigation.

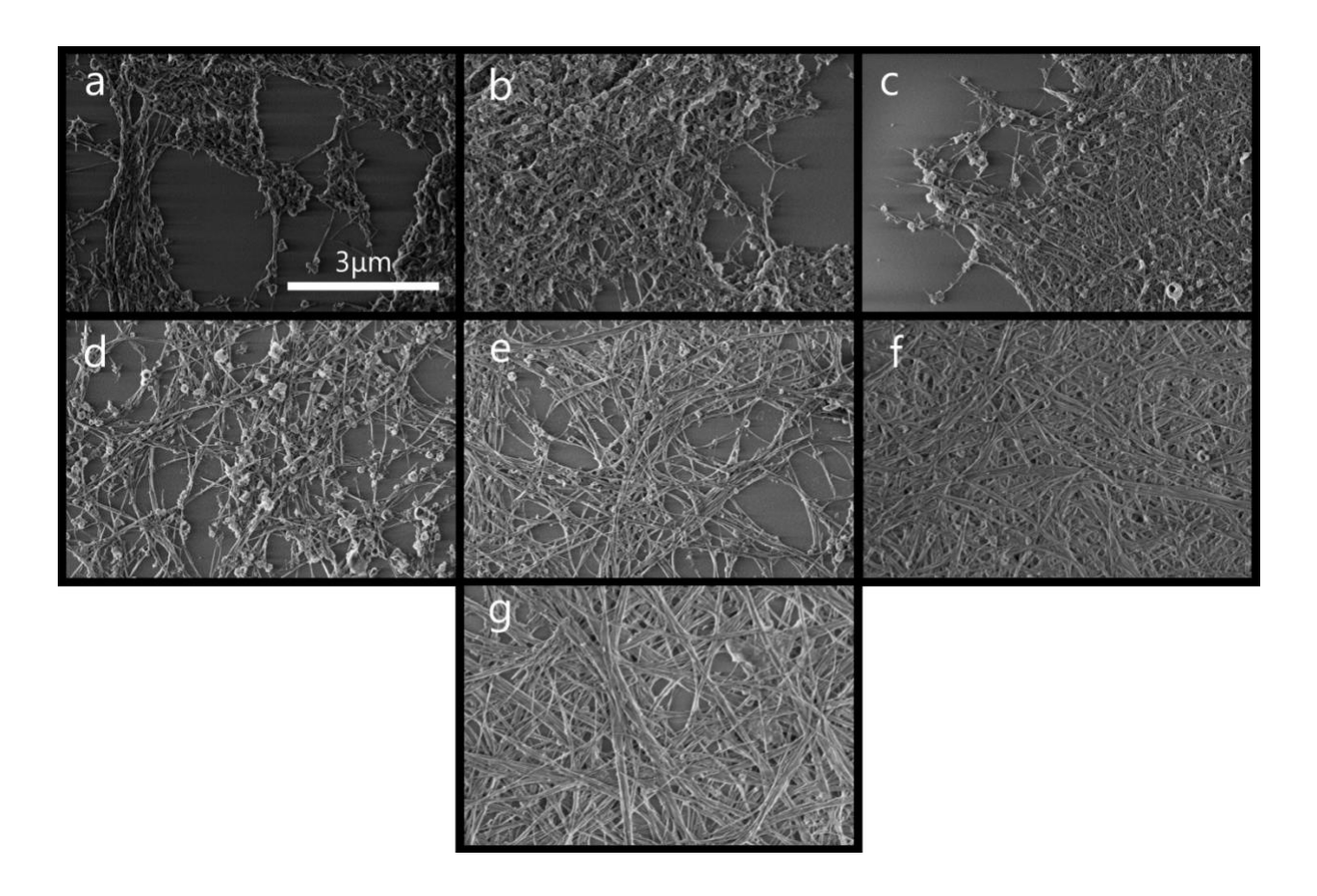


Figure 2. SEM micrographs of time series with HCl•H₃PO₄ BNNT purification in constant volume at 150 °C. (a) 2 hours, (b) 6 hours, (c) 12 hours, (d) 18 hours, (e) 24 hours, (f) 30 hours (g) 36 hours.

The removal of cages from the starting material (Figure 1a, d, g) is remarkable when compared with the purified material (Figure 1c, f, i). The purified material looks tubular with individual tubes or large tube bundles, and a very low concentration of cages (Figure 1c, f, i). In the rare occurrence of cages, there are darkened areas in the centers, which implies that they are etched on that surface. High-resolution, low-current experiments were performed on these samples to confirm that this is not an artifact of charging due to the abundance of electrons in the non-conductive sample (Figure S1). This further supports the asymmetric nature of the etching of non-tube material vs tubes.

TEM was also performed in order to further study cages' preferential etching (Figure 3). While TEM ordinarily would be a good tool to use for characterization of the material, SEM provides a better field of view. As the cages in the starting material are clearly visible in the SEM images, we chose to focus on SEM as a tool for determining bulk enrichment of tubes and tubelike material. TEM images, however, do show that cages are crystalline in the starting material and become etched as the process of purification progresses (Figure 3b,c). Furthermore, tubes were able to be found aggregated with cages in the starting material, but cages were always isolated in the purified material. This suggests that the association of tubes and cages is much stronger when the cages are not damaged.

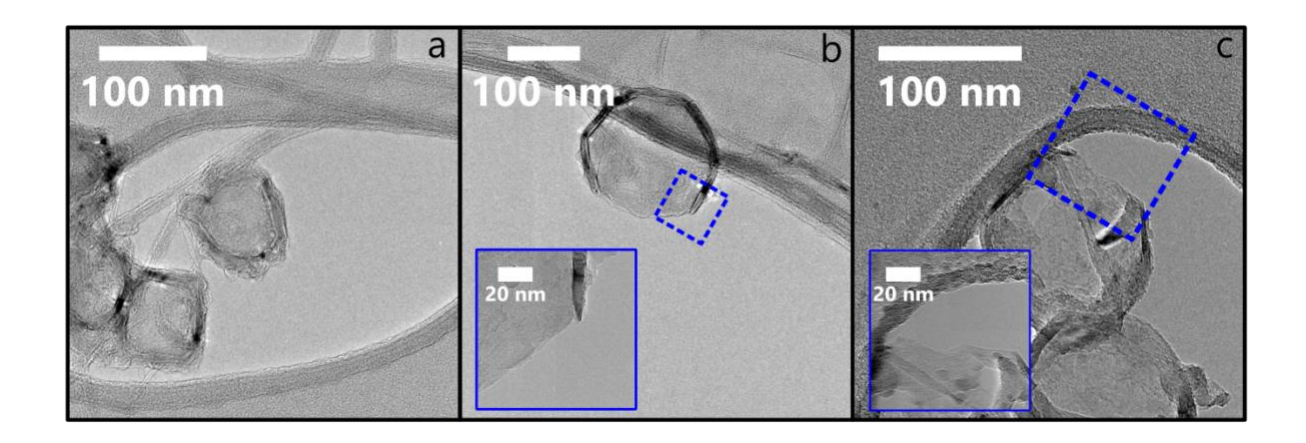


Figure 3. TEM of BNNT samples focused on cage-like structures. (a) Starting material. Tubes are attached to cage-like material, with smaller cages adsorbing to the material. (b) H₃PO₄ BNNT purification in constant volume at 150 °C. Damaged cage is traced in blue. (c) HCl•H₃PO₄ BNNT purification in constant volume at 150 °C. Damaged cage is traced in blue.

Another significant change in morphology of the overall material in the SEM micrographs shown is a terracing effect that happens with the purified material. The base material tends to lay flat on the surface after spin coating. This is likely due to the uniformity of the van der Waals interactions between tubes and cages. Conversely, in the purified material the absence of cages results in long-range ordered domains. These domains can 'stack' better, resulting in the order seen in both the terracing and directionality of the domains.

pH studies were done to elucidate the effects of pH (Figure S5) on the overall purity of the final material. Reactions with phosphoric acid were performed with different pH values from <1 to 8. At pH<1 (which is below pKa₁ of phosphoric acid at 2.12), we found the highest purity. Thus, for a repeatable purification of BNNTs, constant volume reactions at 150 °C for at least 18 hours (or longer with better purity, but lower mass yield) with 0.71 M hydrochloric acid and 4.3 M (25% w/w with water) phosphoric acid, provides the optimal conditions for purification (Figure

2). The edges of tubes and hBN, as well as defects in cages, likely have boric acid moieties, which at low pH can get protonated and hydrolyze creating defects and allowing the coordination of phosphoric acid and formation of boron phosphate. The more defects get produced, the faster the reaction. This is further supported by experiments conducted using organic solvents instead of water. Experiments performed in solvents with a limited amount or no protons, such as methanol, THF and DMF (Figure S6) look similar to experiments at high pH. Alternatively, other acids (HNO₃, HCl, acetic acid, and oxalic acid) do not seem to preferentially etch non-tube vs tube material (Figure S7). It is not clear whether this is a kinetics or thermodynamics issue, though this was not explored further. Finally, a time series was conducted with phosphoric acid (Figure 2) in order to demonstrate the extent to which purity can be obtained at low pH. By 12 hours (Figure 2c), the asymmetric destruction of cages can start to be seen. At 24 hours (Figure 2e), very few cages are left, while at 36 hours (Figure 2g), the highest purity was obtained.

Bulk Characterization

A variety of experiments were performed to characterize the reaction of BNNTs with phosphoric acid. For example, X-Ray diffraction (XRD) was conducted to identify the species formed. Boron phosphate has a characteristic XRD pattern, which is dictated by its crystalline structure. The sample treated with 85% phosphoric acid (Figure 4, purple trace), shows an XRD pattern typical of boron phosphate. On the other hand, BNNTs and other BN nanomaterials do not have a periodic 3-dimensional organization, which results in broad and weak peaks around 26° (Figure 4, red and black traces), with the exception of hBN, which has a sharp peak at 26.75° (Figure 4, blue trace), due to layer stacking. The spacing corresponding to this would be between 3.3 and 4 Å, which is the typical layer distance for stacked BN. Interestingly, the peak in this area for the purified material (Figure 4, green trace) shows a mix of sharp and broad peaks, which is

consistent with previous observations in pure, few-wall carbon nanotubes.³² Also, no diffraction due to boron phosphate was observed in the purified material. It is very likely that the broad peaks observed for the black and red traces are due to the high content of cages, which have a more heterogeneous interlayer distance and the lack of long-range order. The elimination of interstitial material (cages) can lead to a better orientation of tubes and sharpening of that peak.

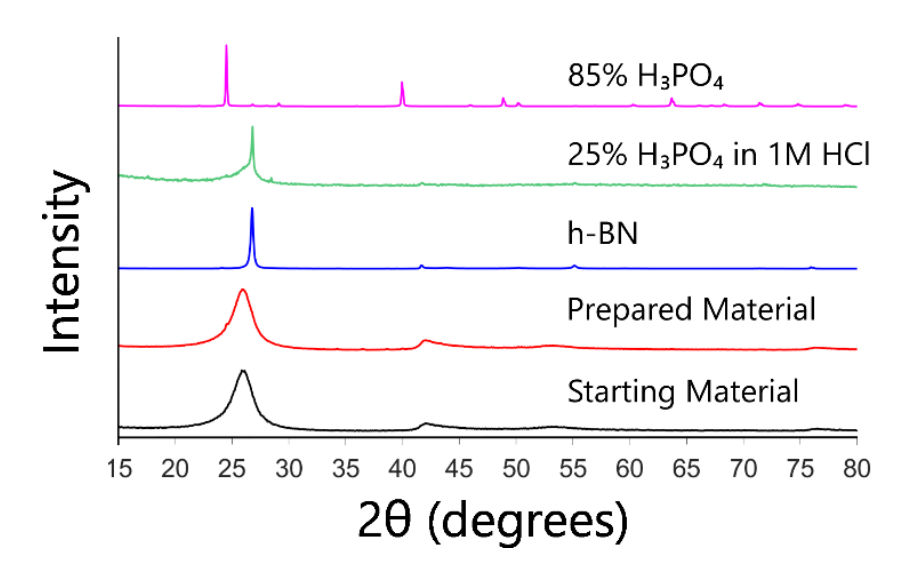


Figure 4. Normalized XRD patterns for BN starting and processed material. Purple trace: 85% phosphoric acid – correspondent to the XRD diffractogram of BPO₄.²⁶ Green trace: purified material; peak at 2θ =26.8. Blue trace: h-BN; peak at 2θ =26.75. Red trace: starting material dispersed in DMF, followed by lyophilization; 2θ =25.9. Black trace: starting material; 2θ =25.9

To further confirm that boron phosphate was removed from the purified material, additional characterization techniques were employed. FTIR was used to verify the identity of the different

functional groups in the materials. The FTIR spectra of the as-received BNNTs, 85% phosphoric acid, and 25% phosphoric acid reactions were obtained and presented in Figure 5. The FTIR samples were normalized to the in-plane BN vibrational mode in order to better compare each sample. The peaks at 1351 cm⁻¹ for both the 25% phosphoric acid-purified, and as-received material overlapped very strongly, with a slight broadening of the purified material peak. Interestingly, the ratio between the 1351 cm⁻¹ (in-plane vibrational mode) and the ca. 795 cm⁻¹ (out-of-plane vibrational mode) does seem to change with purification. This was a common trait among the purified samples, though it is unclear what caused the difference in the ratio.¹⁴ Additionally, the feature around 3250 cm⁻¹ in both the 25% purified and as-received material is due to the oxides of boron present at defect sites. 33-36 While this peak can sometimes be attributed to water adsorption, this is not likely, as all samples were subjected to heating under vacuum prior to analysis in order to remove any water. The concentration of defects decreases in the purified material, which is what is expected from Scheme 1, as part of the removal of defectrich cages. Furthermore, this peak is not present in the 85% phosphoric acid reaction as virtually all the material is converted to BPO₄. Moreover, in the 85% phosphoric acid reaction, the vibrational modes for boron phosphate at ca. 1050 and 910 cm⁻¹ can be seen.³⁰ These correspond to the B-O pseudo lattice translation (910 cm⁻¹) and the P-O vibrational mode (1050 cm⁻¹). BPO₄ assumes an α-cristobalite structure, consisting of alternating boron and phosphorus atoms inside a lattice of oxygen. ^{28,30} It is remarkable from Figure 5 that in the 25% phosphoric acid-purified material, there is no peak at 1050 cm⁻¹ or 910 cm⁻¹ associated with boron phosphate. Therefore, any boron phosphate that is created in the reaction is removed during the washing steps. This is due to the water solubility of amorphous boron phosphate.³⁰

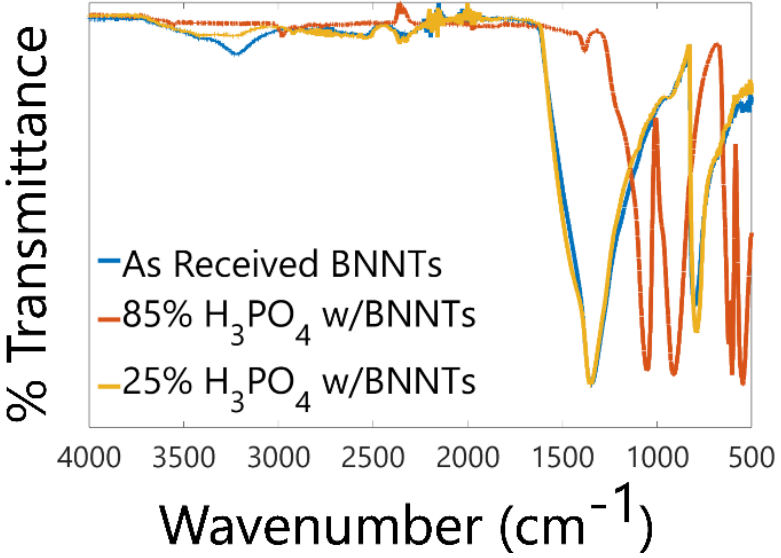


Figure 5. Normalized FTIR spectra for BN starting and processed material.

Another spectroscopic technique used to evaluate the composition of the material is XPS, which provides information about the atomic composition, connectivity, and potential defects in the samples. High-resolution scans portray a boron-to-nitrogen ratio of 0.92:1 for the starting material (Table S1). Similar ratios are obtained for the purified material at 0.97:1 (Table S1). However, the ratio of boron to nitrogen for the 85% phosphoric acid reaction was 34.8:1. This is due to the majority of the nitrogen being converted into ammonia (or soluble nitrogen oxides) during the hydrothermal reaction. These amounts are tabulated in Supporting Information, Table S1. It should be noted that the overlap of the P 2s peak with the B 1s peak has been taken into consideration in each of these calculations.

Deconvolution of XPS data can offer insights into the particular environments present in each sample. Specifically, a peak around 190.5 eV is attributed to the hexagonal bond connectivity of BN that is present in tubes and cages, while a peak around 192.5 eV is attributed to boron-

oxygen bonds in hBN, likely due to defects or edge sites.³⁷ A detailed analysis of the highresolution spectra shows that the B 1s peaks for the as-received and the 25% phosphoric acid purified material both appear at 190.8 eV (Figure 6, middle right), which corresponds to sp² boron bound to nitrogen as in hBN. Interestingly, the purified material has a sharper peak with a lower full-width half maximum, indicating fewer unique binding environments, which implies more homogeneity. Both spectra show peaks around 192.5 eV (Figure 6, middle and bottom right), which correspond to the various boron oxide species, most likely present at the tips of the tubes or defects in the boron nitride material. To determine the content of boron-oxygen species, the peaks around 192.5 eV were analyzed, and a percentage of that contribution was determined. These were then compared to the overall oxygen percentage in the sample to verify that the oxygen is accounted for properly. For instance, in the purified material, the B 1s spectrum shows 14% contribution from boron oxide. This 14% is then taken as a fraction of the total atomic percentage of boron (40.2%) and corresponds to 5.6% of the total atomic percentage. The total atomic percentage of oxygen in the purified material is 4.4%, which is consistent with the B-O percentage.

When comparing the starting and purified material with the 85% phosphoric acid treated material, some key differences arise in the B 1s spectrum. Notably, the signal needs to be deconvoluted into three peaks. For the 191.8 eV maximum (Figure 6, top right), this energy corresponds to the P 2s in BPO₄. There could also be some overlap with the BN signal, but its contribution would be small based on the nitrogen composition (0.8%).

This is confirmed by the SEM image in Figure 1(b, e, h), which indicates very little BN material remaining. Moreover, two distinct peaks appear higher and lower in binding energies at 193.6 and 189.5 eV, respectively (Figure 6, top right). While the 193.6 eV peak can be compared to

the boron oxide peaks in the purified and starting materials, in the 85% phosphoric acid material, this peak is shifted 1 eV to higher energies. Namely, this peak correlates well with the B-O binding energy specific to boron phosphate.²⁵ This area also corresponds to the B₂O₃ binding energy, or other boron oxide species not described above.²⁶

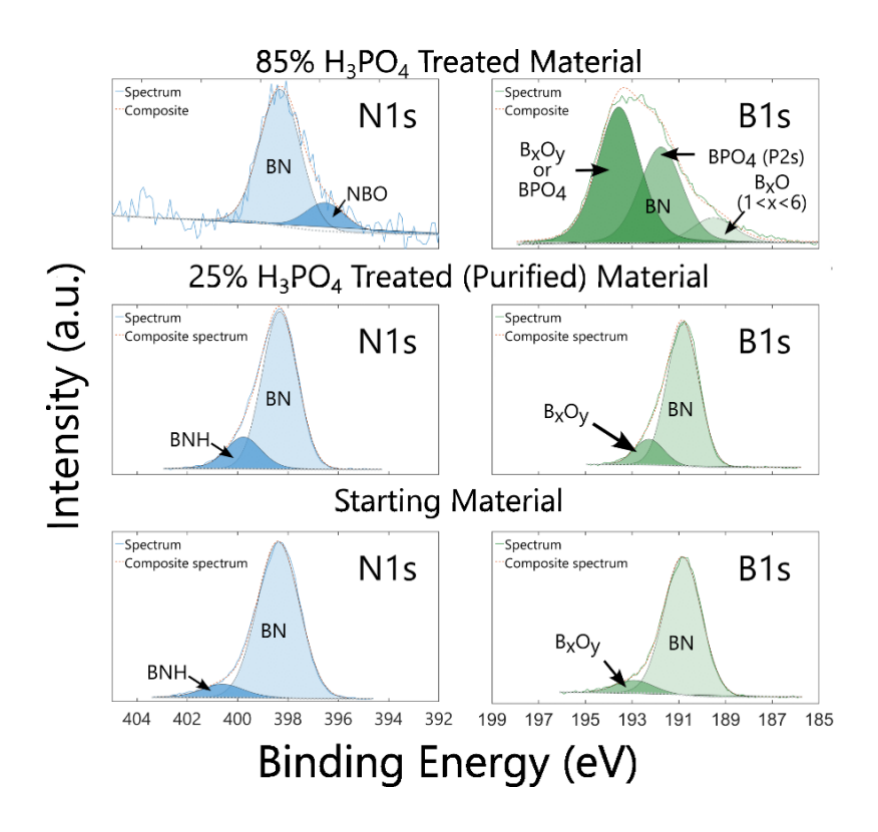


Figure 6. High-resolution XPS scans for starting material, 85% phosphoric acid processed material and 25% H3PO4 in 1 M HCl processed material.

Alternatively, the peak at 189.5 eV had no analog in the purified or starting material. This is a less studied section of boron binding with nitrogen and has been found to correspond to

potentially B-H or B-C.³⁷ Yet, this does not seem likely, given the amount of oxygen present in the 85% phosphoric acid treated material. Instead, this peak is likely attributable to lower boron oxide species that have been associated with the formation of boron suboxide or B₆O. These species are generally formed at high temperature by mixing liquid boron oxide with boron, though some surface materials have been formed more easily.^{38,39} Furthermore, various boron oxides where the boron is higher in concentration than oxygen has been shown to be present in the 188.1 eV area.^{38–42} Conversely, this area may also correspond to the formation of B-P bonds, though this is less likely, as phosphorus was bound to oxygen in the acid.⁴³

The N 1s peaks at 398.3 and 398.4 eV, for the starting and purified material respectively, agree well with one another and correspond to the B-N binding energies, ²⁶ while also agreeing with the 85% phosphoric acid processed material as well (Figure 6, left). However, the latter had less than 1% Nitrogen composition, which implies the complete conversion of nitrogen to gaseous ammonia or to oxidized products that were removed during the washing step. Additionally, for the 85% phosphoric acid treated material, there was a tail present at around 396 eV, which corresponds to nitrogen bound to boron oxide. ⁴⁴ This is likely caused by oxygen being imparted as a result of phosphoric acid coordination/etching and removed from the greater BN structure. Both the purified and starting material also had peaks around 400 eV that are consistent with amine groups, likely at the edges and defects of the BN material.

Finally, the high oxygen amount in the 85% phosphoric acid treated material can be explained by the production of BPO₄, and some boron oxide species. The as-received material and the purified material are very similar in the O 1s spectra, with the starting material having slightly lower percentage of oxygen present; 2.9 and 4.4%, respectively for the as-received and purified

materials. Alternatively, for the 85% phosphoric acid treated material, there was 47.1% oxygen in the sample. This is consistent with the formation of boron phosphate.

Conclusion

Phosphoric acid has been shown to react with boron nitride nanomaterials to form boron phosphate. We have tuned this reaction to remove unwanted BN nanocages from BNNTs that were produced using the HTP method (SP10R). The highest purity material was obtained under these conditions: 3 mg/mL using 25% (4.3 M) phosphoric acid 0.73 M HCl at 150 °C for 24 hrs, with mass yields ranging from 29% to <1% depending on the amount of impurities in the starting material. We propose that the reaction of boron species with phosphoric acid produces amorphous boron phosphate that is washed away in the post-processing steps. Amorphous vs crystalline boron phosphate is produced by decreasing the concentration of phosphoric acid to 25%. BN nanocages get preferentially affected, given their higher reactivity due to a higher concentration of defects. The preferential etching of BN nanocages results in a material that is highly enriched in BNNTs. That said, while this process does preferentially remove non-tube material, the specific ratio of cages to tubes in the starting material does influence the purity and yield of the final product. The higher that ratio, the lower the yield of the final product, as the process removes cages more readily than tubes. Because the concentration of cages in BNNTs is batch-dependent, the material is highly variable, resulting in contaminations that are not homogenous from batch to batch. Therefore, batches with a higher proportion of cages in the starting material might require tuning of the reaction conditions for the complete removal of the cages. With that in mind, due to the small-scale nature of our method and the relatively low cost of materials, this purification process is highly accessible. The method provided here also

demonstrates a significant advance in the purification of BNNTs due to its simplicity, accessibility, and high purity.

Corresponding Author

Angel Martí

*amarti@rice.edu

Author Contributions

 ∇ These authors contributed equally.

Funding Sources

We acknowledge the financial support from the National Science Foundation (CHE-1807737 and CHE-2108838), AFOSR (FA9550-19-1-7045), and The Welch Foundation (Welch C-1668). We thank BNNT LLC, particularly Lyndsey Scammell, for helpful discussions and assistance in procuring material for the study.

Notes

The authors declare no competing financial interest.

Acknowledgments

The authors acknowledge BNNT LLC for providing the boron nitride material. Rice University Shared Equipment Authority provided the equipment used in this study.

ABBREVIATIONS

BNNT, boron nitride nanotubes; CNT, carbon nanotubes; hBN, hexagonal boron nitride; BN, boron nitride; HTP, high-temperature-pressure; DMF, dimethylformamide; SEM, scanning

electron microscopy; FTIR, Fourier transform infrared spectroscopy; XRD, x-ray diffraction; XPS, x-ray photoelectron spectroscopy; H₃PO₄, phosphoric acid; HCl, hydrochloric acid; H₃BO₃, boric acid; B₂O₃, boron oxide; BPO₄, boron phosphate.

Supporting Information

• Limiting charging aberrations with low voltage, high resolution SEM; XPS analysis and collated table; boron phosphate production using hBN, boric acid, and BNNTs under varying conditions; pH, solvent, and acid experiments with SEM images.

References

- (1) Kalay, S.; Yilmaz, Z.; Sen, O.; Emanet, M.; Kazanc, E.; Çulha, M. Synthesis of Boron Nitride Nanotubes and Their Applications. *Beilstein J. Nanotechnol.* **2015**, *6*, 84–102. https://doi.org/10.3762/bjnano.6.9.
- (2) Kim, J. H.; Pham, T. V.; Hwang, J. H.; Kim, C. S.; Kim, M. J. Boron Nitride Nanotubes: Synthesis and Applications. *Nano Convergence* **2018**, *5* (1), 17. https://doi.org/10.1186/s40580-018-0149-y.
- (3) Schnorr, J. M.; Swager, T. M. Emerging Applications of Carbon Nanotubes. *Chem. Mater.* **2011**, *23* (3), 646–657. https://doi.org/10.1021/cm102406h.
- (4) Ruoff, R. S.; Qian, D.; Liu, W. K. Mechanical Properties of Carbon Nanotubes: Theoretical Predictions and Experimental Measurements. *Comptes Rendus Physique* **2003**, *4* (9), 993–1008. https://doi.org/10.1016/j.crhy.2003.08.001.
- (5) Chen, X.; Dmuchowski, C. M.; Park, C.; Fay, C. C.; Ke, C. Quantitative Characterization of Structural and Mechanical Properties of Boron Nitride Nanotubes in High Temperature Environments. *Sci Rep* **2017**, *7* (1), 11388. https://doi.org/10.1038/s41598-017-11795-9.
- (6) Ciofani, G.; Raffa, V.; Menciassi, A.; Cuschieri, A. Cytocompatibility, Interactions, and Uptake of Polyethyleneimine-Coated Boron Nitride Nanotubes by Living Cells: Confirmation of Their Potential for Biomedical Applications. *Biotechnology and Bioengineering* 2008, 101 (4), 850–858. https://doi.org/10.1002/bit.21952.
- (7) Mananghaya, M. R. Titanium-Decorated Boron Nitride Nanotubes for Hydrogen Storage: A Multiscale Theoretical Investigation. *Nanoscale* 2019, 11 (34), 16052–16062. https://doi.org/10.1039/C9NR04578C.
- (8) Simonsen Ginestra, C. J.; Martínez-Jiménez, C.; Matatyaho Ya'akobi, A.; Dewey, O. S.; Smith McWilliams, A. D.; Headrick, R. J.; Acapulco, J. A.; Scammell, L. R.; Smith, M. W.; Kosynkin, D. V.; Marincel, D. M.; Park, C.; Chu, S.-H.; Talmon, Y.; Martí, A. A.; Pasquali, M. Liquid Crystals of Neat Boron Nitride Nanotubes and Their Assembly into Ordered Macroscopic Materials. *Nat Commun* 2022, *13* (1), 3136. https://doi.org/10.1038/s41467-022-30378-5.
- (9) Chopra, N. G.; Luyken, R. J.; Cherrey, K.; Crespi, V. H.; Cohen, M. L.; Louie, S. G.; Zettl, A. Boron Nitride Nanotubes. *Science* 1995, 269 (5226), 966–967. https://doi.org/10.1126/science.269.5226.966.
- (10) Tiano, A. L.; Park, C.; Lee, J. W.; Luong, H. H.; Gibbons, L. J.; Chu, S.-H.; Applin, S.; Gnoffo, P.; Lowther, S.; Kim, H. J.; Danehy, P. M.; Inman, J. A.; Jones, S. B.; Kang, J. H.; Sauti, G.; Thibeault, S. A.; Yamakov, V.; Wise, K. E.; Su, J.; Fay, C. C. Boron Nitride Nanotube: Synthesis and Applications. In *Nanosensors, Biosensors, and Info-Tech Sensors and Systems 2014*; SPIE, 2014; Vol. 9060, pp 51–69. https://doi.org/10.1117/12.2045396.
- (11) Lee, C. H.; Bhandari, S.; Tiwari, B.; Yapici, N.; Zhang, D.; Yap, Y. K. Boron Nitride Nanotubes: Recent Advances in Their Synthesis, Functionalization, and Applications. *Molecules* **2016**, *21* (7), 922. https://doi.org/10.3390/molecules21070922.
- (12) Smith, M. W.; Jordan, K. C.; Park, C.; Kim, J.-W.; Lillehei, P. T.; Crooks, R.; Harrison, J. S. Very Long Single- and Few-Walled Boron Nitride Nanotubes via the Pressurized Vapor/Condenser Method. *Nanotechnology* **2009**, *20* (50), 505604. https://doi.org/10.1088/0957-4484/20/50/505604.
- (13) Cho, H.; Walker, S.; Plunkett, M.; Ruth, D.; Iannitto, R.; Martinez Rubi, Y.; Kim, K. S.; Homenick, C. M.; Brinkmann, A.; Couillard, M.; Dénommée, S.; Guan, J.; Jakubinek, M. B.; Jakubek, Z. J.; Kingston, C. T.; Simard, B. Scalable Gas-Phase Purification of Boron Nitride Nanotubes by Selective Chlorine Etching. *Chem. Mater.* **2020**, *32* (9), 3911–3921. https://doi.org/10.1021/acs.chemmater.0c00144.
- (14) Marincel, D. M.; Adnan, M.; Ma, J.; Bengio, E. A.; Trafford, M. A.; Kleinerman, O.; Kosynkin, D. V.; Chu, S.-H.; Park, C.; Hocker, S. J. A.; Fay, C. C.; Arepalli, S.; Martí, A. A.; Talmon, Y.; Pasquali, M. Scalable Purification of Boron Nitride Nanotubes via Wet Thermal Etching. *Chem. Mater.* 2019, 31 (5), 1520–1527. https://doi.org/10.1021/acs.chemmater.8b03785.

- (15) Choi, J.-H.; Kim, J.; Seo, D.; Seo, Y.-S. Purification of Boron Nitride Nanotubes via Polymer Wrapping. *Materials Research Bulletin* **2013**, *48* (3), 1197–1203. https://doi.org/10.1016/j.materresbull.2012.12.017.
- (16) Lee, S.-H.; Kang, M.; Lim, H.; Moon, S. Y.; Kim, M. J.; Jang, S. G.; Lee, H. J.; Cho, H.; Ahn, S. Purification of Boron Nitride Nanotubes by Functionalization and Removal of Poly(4-Vinylpyridine). *Applied Surface Science* **2021**, *555*, 149722. https://doi.org/10.1016/j.apsusc.2021.149722.
- (17) Kode, V. R.; Thompson, M. E.; McDonald, C.; Weicherding, J.; Dobrila, T. D.; Fodor, P. S.; Wirth, C. L.; Ao, G. Purification and Assembly of DNA-Stabilized Boron Nitride Nanotubes into Aligned Films. *ACS Appl. Nano Mater.* **2019**, *2* (4), 2099–2105. https://doi.org/10.1021/acsanm.9b00088.
- (18) Ko, J.; Kim, H. M.; Moon, S. Y.; Ahn, S.; Im, S. G.; Joo, Y. Highly Pure, Length-Sorted Boron Nitride Nanotubes by Gel Column Chromatography. *Chem. Mater.* **2021**, *33* (12), 4723–4732. https://doi.org/10.1021/acs.chemmater.1c01165.
- (19) Amin, M. S.; Atwater, B.; Pike, R. D.; Williamson, K. E.; Kranbuehl, D. E.; Schniepp, H. C. High-Purity Boron Nitride Nanotubes via High-Yield Hydrocarbon Solvent Processing. *Chem. Mater.* **2019**, *31* (20), 8351–8357. https://doi.org/10.1021/acs.chemmater.9b01713.
- (20) Adnan, M.; Marincel, D. M.; Kleinerman, O.; Chu, S.-H.; Park, C.; Hocker, S. J. A.; Fay, C.; Arepalli, S.; Talmon, Y.; Pasquali, M. Extraction of Boron Nitride Nanotubes and Fabrication of Macroscopic Articles Using Chlorosulfonic Acid. *Nano Lett.* **2018**, *18* (3), 1615–1619. https://doi.org/10.1021/acs.nanolett.7b04335.
- (21) Martinez Rubi, Y.; Jakubek, Z. J.; Chen, M.; Zou, S.; Simard, B. Quality Assessment of Bulk Boron Nitride Nanotubes for Advancing Research, Commercial, and Industrial Applications. *ACS Appl. Nano Mater.* **2019**, *2* (4), 2054–2063. https://doi.org/10.1021/acsanm.9b00057.
- (22) Amin, M. S.; Molin, T. E.; Tampubolon, C.; Kranbuehl, D. E.; Schniepp, H. C. Boron Nitride Nanotube Impurity Detection and Purity Verification. *Chem. Mater.* **2020**, *32* (21), 9090–9097. https://doi.org/10.1021/acs.chemmater.0c03609.
- (23) Kovtyukhova, N. I.; Wang, Y.; Lv, R.; Terrones, M.; Crespi, V. H.; Mallouk, T. E. Reversible Intercalation of Hexagonal Boron Nitride with Brønsted Acids. *J. Am. Chem. Soc.* **2013**, *135* (22), 8372–8381. https://doi.org/10.1021/ja403197h.
- (24) Tiano, A. L.; Gibbons, L.; Tsui, M.; Applin, S. I.; Silva, R.; Park, C.; Fay, C. C. Thermodynamic Approach to Boron Nitride Nanotube Solubility and Dispersion. *Nanoscale* **2016**, *8* (7), 4348–4359. https://doi.org/10.1039/C5NR08259E.
- (25) Okazaki, N.; Takahashi, M.; Murai, H.; Tada, A. XPS Studies of a Boron Phosphate Sample: Unreacted H3BO3 or Its Derivatives on the Surface. *Phosphorus Research Bulletin* **1999**, *9* (0), 63–68. https://doi.org/10.3363/prb1992.9.0_63.
- (26) Moulder, J. F.; Chastain, J. *Handbook of X-Ray Photoelectron Spectroscopy: A Reference Book of Standard Spectra for Identification and Interpretation of XPS Data*; Physical Electronics Division, Perkin-Elmer Corp.: Eden Prairie, Minn., 1992.
- (27) Baykal, A.; Kizilyalli, M.; Toprak, M.; Kniep, R. Hydrothermal and Microwave Synthesis of Boron Phosphate, BPO4. *Turkish Journal of Chemistry* **2001**, *25* (1), 425–432.
- (28) Schmidt, M.; Ewald, B.; Prots, Yu.; Cardoso-Gil, R.; Armbrüster, M.; Loa, I.; Zhang, L.; Huang, Y.-X.; Schwarz, U.; Kniep, R. Growth and Characterization of BPO4 Single Crystals. *Z. anorg. allg. Chem.* **2004**, *630* (5), 655–662. https://doi.org/10.1002/zaac.200400002.
- (29) Wang, R.; Jiang, H.; Gong, H.; Zhang, J. Synthesis of Nanosize BPO4 under Microwave Irradiation. *Materials Research Bulletin* **2012**, *47* (8), 2108–2111. https://doi.org/10.1016/j.materresbull.2012.04.028.
- (30) Chen, S.; Ye, M.; Chen, H.-H.; Yang, X.-X.; Zhao, J.-T. Synthesis and Characterization of Nanostructure BPO4. *J Inorg Organomet Polym* **2009**, *19* (2), 139–142. https://doi.org/10.1007/s10904-008-9245-5.
- (31) Kmecl, P.; Bukovec, P. Boron Phosphate: Its Synthesis, Gradual Crystallisation, and Characterisation of Bulk Properties. *Acta Chimica Slovenica* **1999**, *46* (2), 161–171.

- (32) Futaba, D. N.; Yamada, T.; Kobashi, K.; Yumura, M.; Hata, K. Macroscopic Wall Number Analysis of Single-Walled, Double-Walled, and Few-Walled Carbon Nanotubes by X-Ray Diffraction. *J. Am. Chem. Soc.* **2011**, *133* (15), 5716–5719. https://doi.org/10.1021/ja2005994.
- (33) Harrison, H.; Lamb, J. T.; Nowlin, K. S.; Guenthner, A. J.; Ghiassi, K. B.; Kelkar, A. D.; Alston, J. R. Quantification of Hexagonal Boron Nitride Impurities in Boron Nitride Nanotubes via FTIR Spectroscopy. *Nanoscale Adv.* **2019**, *I* (5), 1693–1701. https://doi.org/10.1039/C8NA00251G.
- (34) Zhang, H.; Shin, B.-G.; Lee, D.-E.; Yoon, K.-B. Preparation of PP/2D-Nanosheet Composites Using MoS2/MgCl2- and BN/MgCl2-Bisupported Ziegler–Natta Catalysts. *Catalysts* **2020**, *10* (6), 596. https://doi.org/10.3390/catal10060596.
- (35) Jiang, H.; Cai, Q.; Mateti, S.; Yu, Y.; Zhi, C.; Chen, Y. Boron Nitride Nanosheet Dispersion at High Concentrations. *ACS Appl. Mater. Interfaces* **2021**, *13* (37), 44751–44759. https://doi.org/10.1021/acsami.1c11795.
- (36) Nautiyal, P.; Loganathan, A.; Agrawal, R.; Boesl, B.; Wang, C.; Agarwal, A. Oxidative Unzipping and Transformation of High Aspect Ratio Boron Nitride Nanotubes into "White Graphene Oxide" Platelets. *Sci Rep* **2016**, *6* (1), 29498. https://doi.org/10.1038/srep29498.
- (37) Guimon, C.; Gonbeau, D.; Pfister-Guillouzo, G.; Dugne, O.; Guette, A.; Naslain, R.; Lahaye, M. XPS Study of BN Thin Films Deposited by CVD on SiC Plane Substrates. *Surface and Interface Analysis* **1990**, *16* (1–12), 440–445. https://doi.org/10.1002/sia.740160191.
- (38) Burke, A. R.; Brown, C. R.; Bowling, W. C.; Glaub, J. E.; Kapsch, D.; Love, C. M.; Whitaker, R. B.; Moddeman, W. E. Ignition Mechanism of the Titanium–Boron Pyrotechnic Mixture. *Surface and Interface Analysis* **1988**, *11* (6–7), 353–358. https://doi.org/10.1002/sia.740110614.
- (39) Ong, C. W.; Huang, H.; Zheng, B.; Kwok, R. W. M.; Hui, Y. Y.; Lau, W. M. X-Ray Photoemission Spectroscopy of Nonmetallic Materials: Electronic Structures of Boron and BxOy. *Journal of Applied Physics* **2004**, *95* (7), 3527–3534. https://doi.org/10.1063/1.1651321.
- (40) Moddeman, W. E.; Burke, A. R.; Bowling, W. C.; Foose, D. S. Surface Oxides of Boron and B12O2 as Determined by XPS. *Surface and Interface Analysis* **1989**, *14* (5), 224–232. https://doi.org/10.1002/sia.740140503.
- (41) Bolmgren, H.; Lundström, T.; Okada, S. Structure Refinement of the Boron Suboxide B6O by the Rietveld Method. In *AIP Conference Proceedings*; AIP: Albuquerque, NM (USA), 1991; Vol. 231, pp 197–200. https://doi.org/10.1063/1.40868.
- (42) Maletaškić, J.; Luković, J.; Yoshida, K.; Yano, T.; Maki, R. S. S.; Gubarevich, A.; Matović, B. High-Temperature Synthesis and Characterization of Boron Suboxide (B6O) and Boron Containing Hard Materials. *Materials Today: Proceedings* **2019**, *16*, 95–101. https://doi.org/10.1016/j.matpr.2019.05.281.
- (43) Mou, S.; Wu, T.; Xie, J.; Zhang, Y.; Ji, L.; Huang, H.; Wang, T.; Luo, Y.; Xiong, X.; Tang, B.; Sun, X. Boron Phosphide Nanoparticles: A Nonmetal Catalyst for High-Selectivity Electrochemical Reduction of CO2 to CH3OH. *Advanced Materials* **2019**, *31* (36), 1903499. https://doi.org/10.1002/adma.201903499.
- (44) Gouin, X.; Grange, P.; Bois, L.; L'Haridon, P.; Laurent, Y. Characterization of the Nitridation Process of Boric Acid. *Journal of Alloys and Compounds* **1995**, *224* (1), 22–28. https://doi.org/10.1016/0925-8388(95)01532-9.